arXiv:1609.06437v1 [quant-ph] 21 Sep 2016

Experimental realization of robust dynamical decoupling with bounded controls in a solid-state spin system

F. Wang[1], C. Zu[1], L. He[1], W.-B. Wang[1], W.-G. Zhang[1], L.-M. Duan[1,2]

[1] *Center for Quantum Information, IIIS, Tsinghua University, Beijing 100084, PR China*
[2] *Department of Physics, University of Michigan, Ann Arbor, Michigan 48109, USA*

(Dated: September 22, 2016)

We experimentally demonstrate a robust dynamical decoupling protocol with bounded controls using long soft pulses, eliminating a challenging requirement of strong control pulses in conventional implementations. This protocol is accomplished by designing the decoupling propagators to go through a Eulerian cycle of the coupler group [*Phys. Rev. Lett. 90, 037901(2003)*]. We demonstrate that this Eulerian decoupling scheme increases the coherence time by two orders of magnitude in our experiment under either dephasing or a universal noise environment.

PACS numbers:

INTRODUCTION

Dynamical decoupling is a powerful method to combat decoherence of quantum systems caused by coupling to slow-varying environment [1–8]. Conventional dynamical decoupling requires to apply a sequence of strong instantaneous pulses [1, 5, 8], with the pulse duration shorter than other time scales in the system so that the control sequence can be approximated by δ-pulses or unbounded control Hamiltonians. Decoupling schemes based on finite-width pulses, such as the magic-echo trains, have been proposed and implemented in experiments [9, 10], however, they still require the driving amplitude to be much higher than other dynamical parameters in the system [10]. Dynamical decoupling has been used in a number of quantum information systems to suppress decoherence, with particular applications to the solid state spin qubits [11–17]. As any control Hamiltonian in real systems always has bounded parameters, the need of strong pulses with amplitudes larger than other dynamical parameters may impose a serious restriction on applications of the dynamical decoupling method. Theoretically, a method called the Eulerian decoupling scheme has been proposed to overcome this problem [6]. The Eulerian decoupling is highly robust to variation in the pulse length and shape as long as the integral of the pulse completes a π-rotation on the target spin, eliminating the challenging requirement on the pulse amplitude or duration.

In this paper, we report an experimental demonstration of effectiveness of the Eulerian decoupling scheme. We test performance and robustness of the Eulerian decoupling under various noise environments, using the solid-state spin qubits carried by the Nitrogen-Vacancy (NV) centers in a diamond sample. Recently, the NV centers in the diamond have stood out as a promising system for realization of quantum information processing [18–28, 31]. The coherence of this system can be well controlled and manipulated even at room temperature [18–20]. Here, we use this system as a testbed for various dynamical decoupling protocols and show that the Eulerian decoupling scheme with long soft pulses is almost equally effective as the conventional schemes based on strong instantaneous pulses. The natural nuclear spin environment around the diamond NV centers provides a source of dephasing noise. To study the effectiveness of the Eulerian decoupling scheme under general noise including both dephasing and relaxation, we realize a general noise model by injecting microwave noise. Under various noise models, we demonstrate that the corresponding Eulerian decoupling scheme can increase the coherence time of the system by two orders of magnitude in our experiment. The demonstration of effectiveness of the Eulerian decoupling scheme may stimulate applications of this powerful method to systems where strong control pulses are hard to achieve compared with the system-environment coupling rate.

RESULTS

Eulerian decoupling

In the dynamical decoupling scheme, the control Hamiltonian is denoted by $H_c(t)$ with its corresponding propagator given by the time-ordered integration $U_c(t) = \mathscr{T} exp\{-i\int_0^t dt' H_c(t')\}$. In the conventional scheme based on instantaneous pulses, the propagator $U_c(t)$ suddenly changes from g_{l-1} to g_l by the pulse l ($l = 1, 2, \cdots, L$) with $U_c((l-1)t_\Delta + s) = g_{l-1}$ for $0 \le s < t_\Delta$, where t_Δ denotes the time segment between adjacent pulses and the whole control cycle consists of L pulse with total time Lt_Δ. The evolution operators $\{g_l, l = 1, \cdots, L\}$ form a group G and

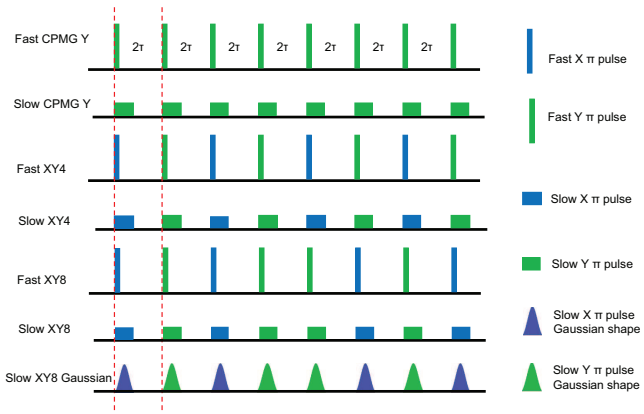

FIG. 1: Dynamical decoupling sequences implemented in our experiments. Each rectangle corresponds to a π rotation of the electron spin. The height and the width of the rectangle correspond to the strength and time duration of the pulse, respectively. The pulse interval 2τ and the pulse duration τ_d together make a complete period with $\tau_c = 2\tau + \tau_d$, which is kept to be the same for different decoupling sequences in our comparison of their performance.

the dynamical decoupling works as we require the system-environment coupling Hamiltonian is averaged out to zero over this group G. For the Eulerian decoupling scheme, the instantaneous pulse is replaced by any continuous pulse which satisfies the condition $U_c\left(lt_\Delta\right) = g_l$. For the Eulerian decoupling scheme to work, $U_c\left(lt_\Delta\right)$ $(l = 1, \cdots, L)$ over one complete control cycle has to follow the so-called Eulerian path in the graph with $\{g_l\}$ as the vertices. If the noise is purely dephasing (Z error), the simplest Eulerian path is given by $\{X, I\}$, which corresponds to the conventional Car-Purcell-Meiboom-Gill (CPMG) echo pulse sequence $\{X, X\}$. We use X, Y, Z in this paper to denote the three Pauli operators. So the CPMG sequence should work for the dephasing noise even when we replace the instantaneous π-pulse by a slow pulse as long as the pulse area is π for each control segment. If the noise is universal including both dephasing and relaxation (X, Y, Z errors), the simplest decoupling sequence with instantaneous pulses is the XY4 sequence $\{X, Y, X, Y\}$. The simplest Eulerian path in this case, however, is given by $\{X, -iZ, -Y, -I, -Y, -iZ, X, I\}$, which corresponds to the XY8 pulse sequence $\{X, Y, X, Y, Y, X, Y, X\}$. According to the Eulerian decoupling scheme, the XY8 sequence should work for any slow pulse of arbitrary shape as long as the pulse area integrated over the duration t_Δ is π for each segment.

Test of Eulerian decoupling under dephasing

In our experiment, we use the electron spin qubit of a NV center in a single crystal diamond to test effectiveness of the Eulerian decoupling scheme. Our experimental setup is described in detail in Ref. [28] and the appendix. We compare the performance of various pulse sequences under both dephasing and universal noise. The pulse sequences tested in this paper are shown in Fig. 1. Note that we use the CPMG Y sequence $\{Y, Y\}$ instead of the X sequence to combat the dephasing noise (Z error) as the Y sequence is more robust to the systematic X error if we prepare and measure the superposition state with X pulses in the Ramsey measurement scheme. The dephasing noise in our experiment is provided by the natural coupling of the electron spin to the surrounding nuclear spins in the diamond crystal, which induces dephasing with $T_2^* \approx 1.85\ \mu s$ measured through the free induction decay under an external magnetic filed of 500 G applied along the NV axis (shown in Fig. 2a). To simulate an environment of universal noise, we apply to the electron spin a noisy microwave field synthesized through an arbitrary waveform generator (AWG) with the details shown in the appendix.

We test effectiveness of the Eulerian decoupling scheme by measuring the coherence decay of the electron spin under different dynamical decoupling pulse sequences, with both fast and slow pulses. We prepare the initial state in the superposition of $|0\rangle$ and $|-1\rangle$ spin state by a $\pi/2$ pulse along the X axis and then let it evolve with the decoupling protocol for a total time duration of $N\tau_c$ (including $\tau_c/2$ before the first pulse and $\tau_c/2$ after the last pulse of the dynamical decoupling sequence), where N is the pulse number and τ_c is the periodic pulse spacing. The performance of the dynamical decoupling is characterized by projecting the final state ρ to the Z axis by another $\pi/2$ pulse along the $-X$ axis and measuring the state fidelity $F = \langle 0|\rho|0\rangle$, which is calibrated by the fluorescence contrast in a Rabi oscillation experiment.

We start by exploiting the Eulerian decoupling protocol under pure dephasing. In Fig. 2, we show the comparison

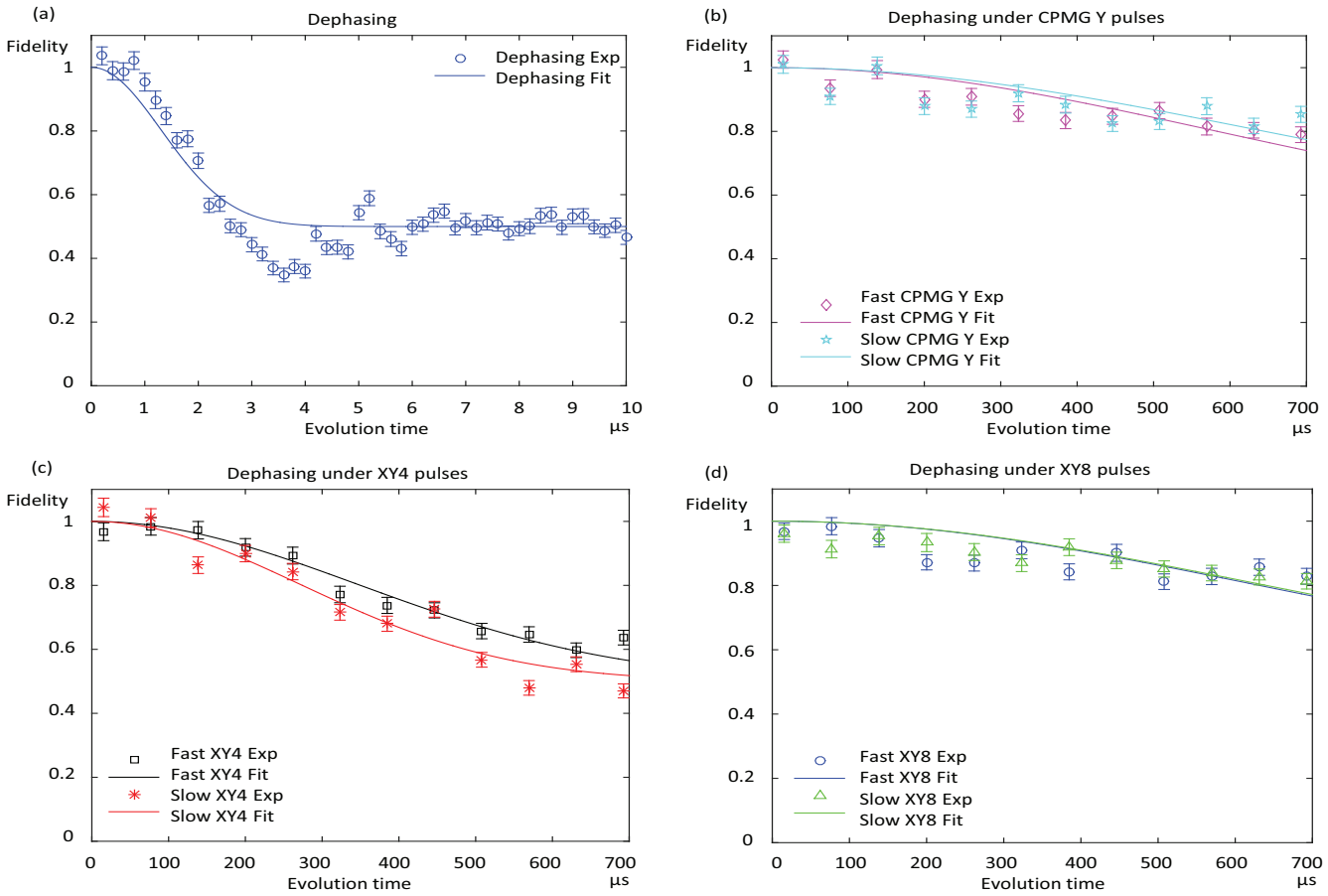

FIG. 2: Coherence decay with the initial states along the $+Y$ axis under pure dephasing. (a) Free induction decay probed using Ramsey interference. Solid line is a fit to $exp(-(t/T_2^*)^2)$ with the fitted $T_2^* = 1.85\ \mu s$. (b,c,d) Coherence decay under repeated CPMG Y (b), XY4 (c), and XY8 (d) dynamical decoupling sequences compared between fast and slow pulses, where the pulse period is fixed and the pulse number N varies from 8 to 360 along the horizontal axis. Solid lines are fits to $exp(-(t/T_2)^2)$ with (b) $T_2 = 816\ \mu s$ ($903\ \mu s$) for the fast (slow) CPMG pulses, (c) $T_2 = 490\ \mu s$ ($384\ \mu s$) for the fast (slow) XY4 pulses, and (d) $T_2 = 884\ \mu s$ ($896\ \mu s$) for the fast (slow) XY8 pulses. The pulse duration τ_d and the pulse interval 2τ are taken to be 24 ns (500 ns) and 1900 ns (1424 ns), respectively, for the fast (slow) pulses.

of performance under fast and slow pulses. Note that under pure dephasing, the CMPG-Y, the XY4, and the XY8 sequences all satisfy the Eulerian cycle condition, so theory predicts these sequences should all work with long pulses instead of strong instantaneous ones. In Fig. 2(b)-(d), we report experimental results with the pulse duration extended to 500 ns, comparable with the pulse interval 2τ ($\tau = 712$ ns) and T_2^*. Compared with the fast pulse case (for which the pulse duration is 24 ns), the Eulerian decoupling sequences with slow pulses give almost the same performance. For all the cases, the coherence time is extended to be hundreds of T_2^*, in agreement with the prediction of the Eulerian decoupling scheme under pure dephasing.

Test of Eulerian decoupling under general noise

Universal noise provides a more interesting environment to test performance of the Eulerian decoupling protocol. To realize a universal noise environment, in addition to intrinsic dephasing in the diamond, we introduce spin relaxation noise by injecting a noisy microwave field. In Fig. 3a and 3b, we characterize the universal noise environment by measuring the spin relaxation and dephasing times under no dynamical decoupling pulses. The magnitude of the noisy microwave filed is controlled such that the corresponding spin relaxation time (T_1^*) is about 10 μs from numerical simulation of the noise model (insert of Fig. 3a). In experiment, however, we observe that the spin population only relax by 20% after 700 μs as shown in Fig. 3a. The observed effect can be explained by the dephasing induced

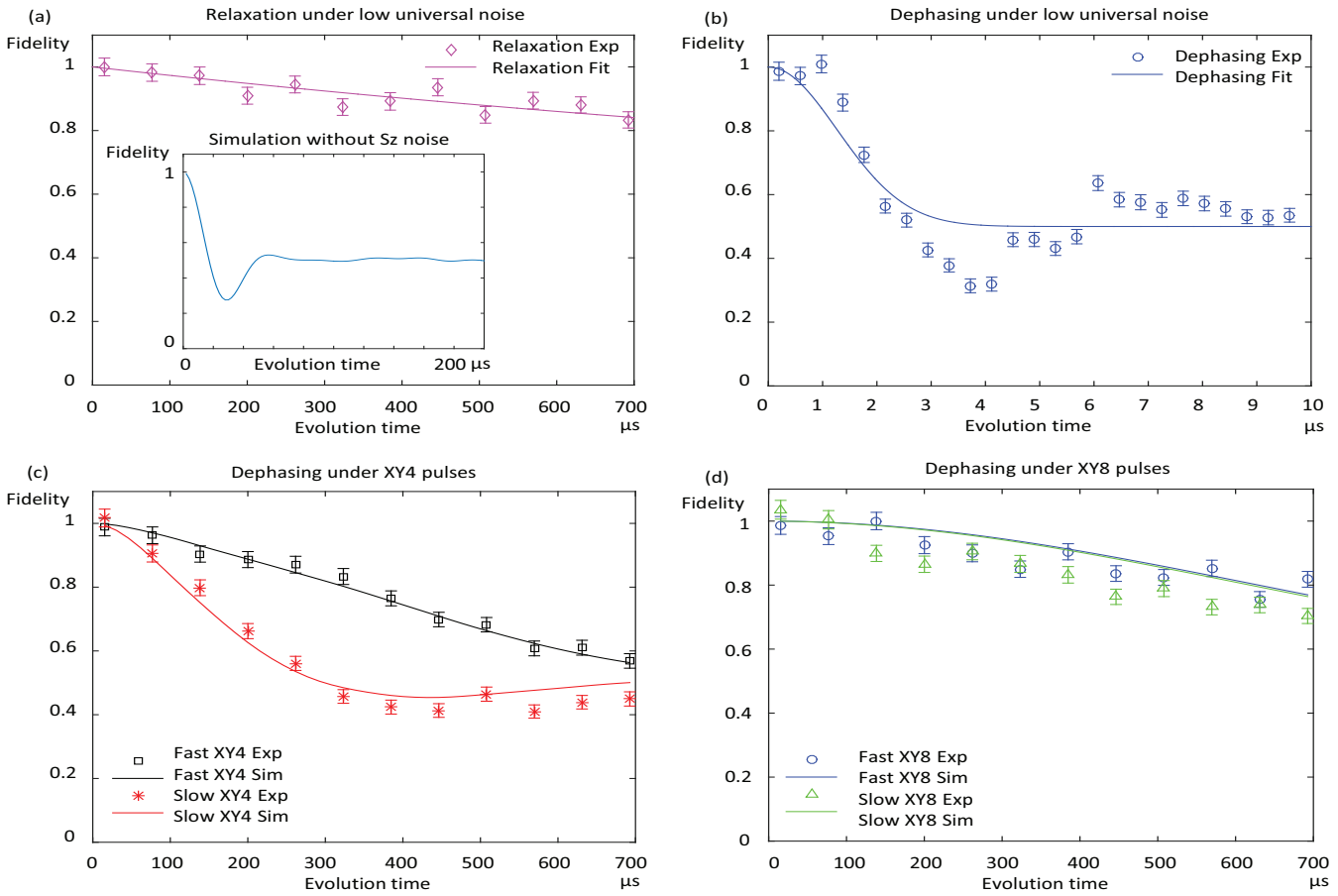

FIG. 3: Coherence decay with the initial states along the $+Y$ axis under weak relaxation environment. (a) Relaxation of spin population in $|0\rangle$ state. Solid line is a fit to $exp(-t/T_1^*)$ with the fitted $T_1^* = 1.83$ ms. The inset shows the numerical simulation result of relaxation with the injected microwave noise if there were no dephasing in the environment, for which $T_1^* = 12.87$ μs. (b) Free induction decay measured with Ramsey interference. Solid line is a fit to $exp(-(t/T_2^*)^2)$ with the fitted $T_2^* = 1.79$ μs. (c,d) Coherence decay under repeated XY4 (c) and XY8 (d) dynamical decoupling sequences compared between fast and slow pulses, where the pulse period is fixed and the pulse number N varies from 8 to 360 along the horizontal axis. Solid lines are numerical simulation results under the injected spin relaxation noise and the natural dephasing environment characterized in Fig. 2 (see the Appendix for the simulation method). The pulse duration τ_d and the pulse interval 2τ are taken to be 24 ns (500 ns) and 1900 ns (1424 ns), respectively, for the fast (slow) pulses.

inhabitation of relaxation [29, 30]. The strong intrinsic dephasing is equivalent in role to frequent observation of population, which freezes population transfer by the noisy microwave field when the magnitude of the latter is small compared with the dephasing rate [29, 30]. Strong dephasing therefore suppresses spin relaxation.

Although the added spin relaxation noise changes little the observed T_1^* and T_2^* in Fig. 3a and 3b, it significantly affects the performance of the dynamical decoupling pulses. Under a universal noise environment, theory predicts that both XY4 and XY8 sequence should work under fast pulses, but only the XY8 sequence, which is the minimum Eulerian decoupling sequence, will work under slow pulses. In Fig. 3c and 3d, we show the performance of the XY4 and the XY8 sequences under both slow and fast pulses. We see that under the XY8 sequence slow pulses achieve almost the same performance as the fast pulses, while under the XY4 sequence the performance of the slow pulses is significantly worse than that of the fast pulses. These observations are in agreement with prediction of the Eulerian decoupling theory.

We then increase the spin relaxation noise by raising the magnitude of the noisy microwave filed and test the performance of the Eulerian decoupling scheme under strong relaxation and dephasing. The results are shown in Fig. 4. In Fig. 4a and 4b, we see that both T_1^* and T_2^* are now reduced to about 1 μs. In Fig. 4c and 4d, we compare the performance of the XY4 and XY8 sequences under slow and fast pulses with the following two observations: First, we note that the overall coherence time becomes shorter, and the XY4 sequence is significantly inferior to the

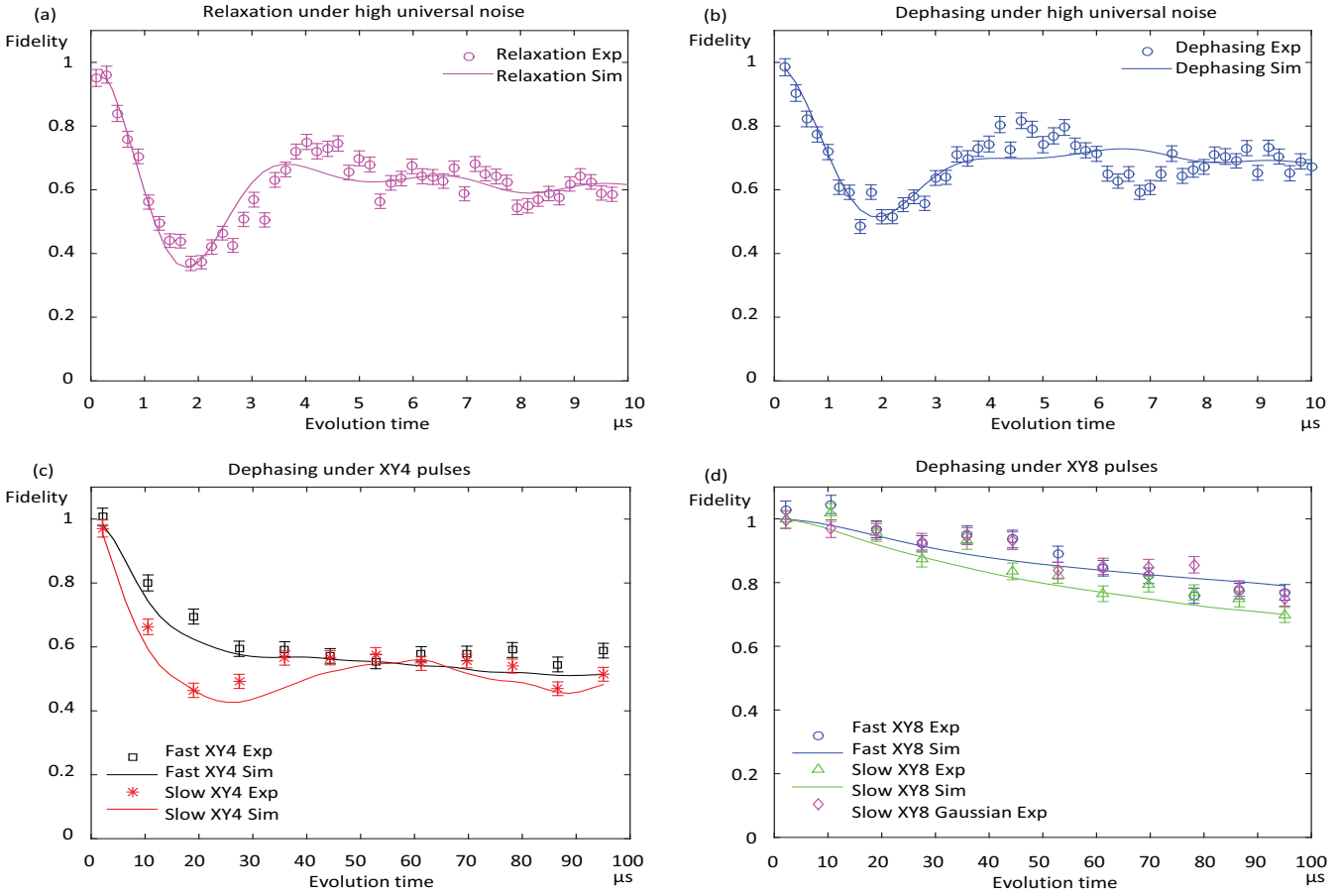

FIG. 4: Same as Fig.3, but under strong relaxation environment. Solid lines represent numerical simulation results (see the Appendix for the simulation method). The pulse duration τ_d and the pulse interval 2τ are taken to be 24 ns (100 ns) and 240 ns (164 ns), respectively, for the fast (slow) pulses.

XY8 sequence in performance even under fast pulses. This is caused by the requirement of a smaller pulse period τ_c in this case and thus fast accumulation of the systematic pulse errors. As it is well known, the XY8 sequence is more insensitive to accumulation of the systematic pulse errors compared with the XY4 sequence as it suppresses the systematic errors and the spin relaxation noise to a higher order [12, 16]. Under pure dephasing, the pulse period τ_c is required to be small compared with the bath correlation time; while under both dephasing and relaxation, the pulse period τ_c needs to be small compared with the time scale of T_1^* and T_2^* (the inverse of the relaxation and the dephasing rates). The latter sets a more stringent requirement and we need to reduce τ_c by about a factor of 8 in our experiment. The overall coherence time correspondingly decreases under the same number of pulses. Second, for the XY4 sequence the fast pulses significantly outperform the slow pulses, while for the XY8 sequence they give similar results. This is in agreement with prediction of the Eulerian decoupling theory. In Fig. 4d, we also test performance of the slow pulses under different pulse shapes, for instance, with a Gaussian instead of a square shape, and find that the slow pulses under different shapes all give very similar results, with performance comparable to that of fast instantaneous pulses.

SUMMARY

In summary, we have reported an experimental test of the Eulerian dynamical decoupling scheme in a solid state spin system and find that the slow soft pulses, under appropriate conditions, are able to give noise suppression comparable to the performance of strong instantaneous pulses. The experimental demonstration of the Eulerian decoupling scheme with slow pulses and its effectiveness eliminates a challenging requirement in conventional dynamical decoupling techniques and may find important applications in physical systems where the system-environment coupling is large

and it is difficult to apply strong control pulses with amplitudes much higher than any other system or environment dynamical parameters [8].

APPENDIX

Experimental Setup

We use a home-built confocal microscopy to optically address single NV centers in the diamond. A 532 nm green laser, controlled by an acoustic optical modulator (AOM), is used for initialization and readout of single NV centers. The AOM is set in a double pass configuration to enhance the on-off ratio to 100000 : 1. The green laser is then coupled into a single mode fiber for optical mode shaping. The laser coming out of the fiber is reflected by a wave length dependent Dichroic Mirror (DM) and focused by an oil immersed objective lens into the diamond sample, which is mounted on a 3-axis closed-loop piezo. The fluorescence of the NV center is collected by the same objective, then passes through the DM mirror and gets collected by a single photon detector with a 637 nm long pass filter.

The spatial resolution of the confocal microscopy system is limited by the diffraction limit of the green laser and the Numerical Aperture (NA) of the objective to about 0.2 μm. The fluorescence count of single NV center is about 100 k/second (the dark count rate is 5 k/second). To collect enough data in experiments, we repeat each experimental trial 10^6 times. We apply a magnetic field of 500 G along the NV axis. Under this filed, the green pumping laser polarizes the nearby N^{14} and C^{13} nuclear spins through the electron spin level anti-crossing in the excited-state manifold, which facilitates electron-spin nuclear-spin flip-flop process during optical pumping [1].

We fabricate a coplanar waveguide transmission line with a 70 μm gap on a cover glass to deliver microwave signal. The microwave signal is first generated in a microwave source, then modulated at an IQ mixer with the output of a frequency combiner, whose input is generated by two separate Arbitrary Wave Generators (AWG). The first AWG generates a 100 MHz signal used to manipulate the electron spin (resonant with the energy level between the $|0\rangle$ and $|-1\rangle$ states after mixed with the microwave output). The second AWG generates the noise signal with a center frequency same as the output of the first AWG and a particular bandwidth corresponding to the interested noise model. The synchronization and on-off of the second AWG is controlled by the digital output of the first AWG via a switch.

Realization of a universal noise model by injecting microwave noise

The intrinsic decoherence in the diamond only provides the dephasing noise. To model a universal noise environment, we need to add spin relaxation, which is achieved by injecting microwave noise to drive the NV spin transitions. The noise signal, after mixed with the microwave output, is centered at the frequency that is resonant with the transition from the level $|0\rangle$ to $|-1\rangle$. To model the relaxation noise, we add up all the frequency components around the center frequency up to a cutoff bandwidth (the bandwidth is taken to be 20 kHz in our experiment) and weight the frequency components with a particular spectrum. To have a time correlation function of the shape $exp(-R|\tau|)$, we choose the weight function to be $\sqrt{\frac{2\Delta\omega R}{(2\pi n\Delta\omega)^2+R^2}}$ for the nth component of the microwave noise field with frequency detuning $n\Delta\omega$, where $\Delta\omega = 1$ kHz is the discretization step. The phase of each frequency component is chosen randomly from a uniform distribution between 0 and 2π. We generate a 1 ms time trace of this spectrum and set the AWG to continuously repeat this 1 ms signal. All the dynamical decoupling sequence is shorter than 1 ms, so the noise has no correlation within a cycle. We have the noise on during the desired evolution period.

Numerical Simulation

Since most of the strong nuclear spins are polarized under optical pumping with a strong magnetic field at 500 Gauss, we ignore the interactions of the electron spins with the nearby nuclear spins. The pulse period τ_c is carefully chosen to avoid the collapse of coherence due to resonance with the 0.5 MHz Larmor precession induced by the external magnetic field. We consider the effective spin-1/2 system composed of $|0\rangle$ and $|-1\rangle$ states. The numerical simulation is performed in the rotating frame using the 4th order Runge-Kutta integration with the effective Hamiltonian given by $H = \Omega cos(\phi)S_x + \Omega sin(\phi)S_y + H_{injectednoise}(t)$, where Ω and ϕ are respectively the Rabi frequency and the phase of the microwave pulses for the dynamical decoupling sequence, and

$H_{injectednoise}(t) = \sum_{n=-10}^{10} W(n)cos(n\Delta\omega t + \phi_n)S_x - W(n)sin(n\Delta\omega t + \phi_n)S_y$ with $W(n) = \sqrt{\frac{2\Delta\omega R}{(2\pi n\Delta\omega)^2+R^2}}$ and random phase ϕ_n simulates the injected microwave noise responsible for the spin relaxation. We perform an average over 1000 realizations of different $H_{injectednoise}(t)$ with random phase ϕ_n in each run. The simulation result is then enveloped with the function $0.5exp(-(t/T_2)^2) + 0.5$ that represents the intrinsic dephasing in the diamond, where T_2 is experimentally measured under the CPMG Y sequence.

This work was supported by the Ministry of Education of China through its grant to Tsinghua University. LMD acknowledges in addition support from the IARPA program, the ARL, and the AFOSR MURI program.

[1] L. Viola and S. Lloyd, Phys. Rev. A 58, 2733 (1998).
[2] P. Zanardi, Phys. Lett. A 258, 77 (1999).
[3] L.-M. Duan and G. Guo, Phys. Lett. A 261, 139 (1999).
[4] D. Vitali and P. Tombesi, Phys. Rev. A 59, 4178 (1999).
[5] L. Viola, E. Knill, and S. Lloyd, Phys. Rev. Lett. 82, 2417 (1999).
[6] L. Viola and E. Knill, Phys. Rev. Lett. 90, 037901 (2003).
[7] K. Khodjasteh and D. A. Lidar, Phys. Rev. Lett. 95, 180501 (2005).
[8] H. K. Ng, D. A. Lidar, J. Preskill, Phys. Rev. A 84, 012305 (2011).
[9] W-K. Rhim, A. Pines, and J. S. Waugh, Phys. Rev. B 3, 684 (1971).
[10] G. S. Boutis, P. Cappellaro, H. Cho, C. Ramanathan, and D. G. Cory, J. Magnetic Resonance 161, 132 (2003).
[11] C. Ryan, J. Hodges, and D. Cory, Phys. Rev. Lett. 105, 200402 (2010).
[12] G. de Lange, Z. H. Wang, D. Riste, V. V. Dobrovitski, R. Hanson, Science 330, 60 (2010).
[13] Boris Naydenov, Florian Dolde, Liam T. Hall, Chang Shin, Helmut Fedder, Lloyd C. L. Hollenberg, Fedor Jelezko, and Jorg Wrachtrup, Phys. Rev. B 83, 081201(R) (2011).
[14] Zhi-Hui Wang, Wenxian ZHang, A. M. Tyryshkin, S. A. Lyon, J. W. Ager, E. E. Haller, and V. V. Dobrovitski, Phys. Rev. B 85, 085206 (2012).
[15] David M. Toyli, Charles F. de las Casas, David J. Christle, Viatcheslav V. Dobrovitski, and David D. Awschalom, PNAS 110, 8417 (2013).
[16] D. Farfurnik, A. Jarmola, L. M. Pham, Z. H. Wang, V. V. Dobrovitski, R. L. Walsworth, D. Budker, and N. Bar-Gill, Phys. Rev. B 92, 060301 (2015).
[17] Wenchao Ma, Fazhan Shi, Kebiao Xu, Pengfei Wang, Xiangkun Xu, Xing Rong, Chenyong Ju, Chang-Kui Duan, Nan Zhao, and Jiangfeng Du, Phys. Rev. A 92, 033418 (2015).
[18] Marcus W. Doherty, Neil B. Manson, Paul Delaney, Fedor Jelezko, Jorg Wrachtrup, Lloyd C. L. Hollenberg, Physics Reports 528, 1 (2013).
[19] L. Childress, R. Walsworth, and M. Lukin, Physics Today 67, 38 (2014).
[20] F. Jelezko, T. Gaebel, I. Popa, A. Gruber, and J. Wrachtrup, Phys. Rev. Lett. 92. 076401 (2004).
[21] P. Neumann, N. Mizuochi, F. Rempp, P. Hemmer, H. Watanabe, S. Yamasaki, V. Jacques, T. Gaebel, F. Jelezko, J. Wrachtrup, Science 320, 1326 (2008).
[22] V. Jacques, P. Neumann, J. Beck, M. Markham, D. Twitchen, J. Meijer, F. Kaiser, G. Balasubramanian, F. Jelezko, and J. Wrachtrup, Phys. Rev. Lett. 102, 057403 (2009).
[23] N. Y. Yao, L. Jiang, A. V. Gorshkov, P. C. Maurer, G. Giedke, J. I. Cirac and M. D. Lukin, Nature Commun. 3, 800 (2012).
[24] T. van der Sar, Z. H. Wang, M. S. Blok, H. Bernien, T. H. Taminiau, D. M. Toyli, D. A. Lidar, D. D. Awschalom, R. Hanson, and V. V. Dobrovitski, Nature 484, 82 (2012).
[25] P. C. Maurer, G. Kucsko, C. Latta, L. Jiang, N. Y. Yao, S. D. Bennett, F. Pastawski, D. Hunger, N. Chisholm, M. Markham, D. J. Twitchen, J. I. Cirac, M. D. Lukin, Science 336, 1283 (2012).
[26] Florian Dolde, Ville Bergholm, Ya Wang, Ingmar Jakobi, Boris Naydenov, Sebastien Pezzagna, Jan Meijer, Fedor Jelezko, Philipp Neumann, Thomas Schulte-Herbruggen, Jacob Biamonte, and Jorg Wrachtrup, Nature Comm. 5, 3371 (2014).
[27] W. Pfaff, B. J. Hensen, H. Bernien, S. B. van Dam, M. S. Blok, T. H. Taminiau, M. J. Tiggelman, R. N. Schouten, M. Markham, D. J. Twitchen, R. Hanson, Science 345, 532 (2014).
[28] C. Zu, W. -B. Wang, L. He, W. -G. Zhang, C. -Y. Dai, F. Wang and L. -M. Duan, Nature 514, 72 (2014).
[29] N. Syassen, D. M. Bauer, M. Lettner, T. Volz, D. Dietze, J. J. Garcia-Ripoll, J. I. Cirac, G. Rempe, S. Durr, Science 320, 1329 (2008).
[30] Y.-J. Han, Y.-H. Chan, W. Yi, A. J. Daley, S. Diehl, P. Zoller, L.-M. Duan, Phys. Rev. Lett. 103, 070404 (2009).
[31] B. Hensen, H. Bernien, A. E. Dreau, A. Reiserer, N. Kalb, M. S. Blok, J. Ruitenberg, R. F. L. Vermeulen, R. N. Schouten, C. Abellan, W. Amaya, V. Pruneri, M. W. Mitchell, M. Markham, D. J. Twitchen, D. Elkouss, S. Wehner, T. H. Taminiau, and R. Hanson, Nature 526, 682-686 (2015).
[32] V. Jacques, P. Neumann, J. Beck, M. Markham, D. Twitchen, J. Meijer, F. Kaiser, G. Balasubramanian, F. Jelezko, and J. Wrachtrup, Phys. Rev. Lett. 102, 057403(2009).